JOURNAL OF GEOPHYSICAL RESEARCH, VOL. 101, NO. A10, PAGES 21,731–21,741, OCTOBER 1, 1996

Auroral emission profiles extracted from three-dimensionally reconstructed arcs

S. Frey and H. U. Frey

Max-Planck-Institut für Extraterrestrische Physik, Garching, Germany

D. J. Carr

Research Systems, Inc., Boulder, Colorado

O. H. Bauer and G. Haerendel

Max-Planck-Institut für Extraterrestrische Physik, Garching, Germany

Abstract. The mathematics of emission-computed tomography is applied to the analysis of stereoscopic observations of auroral arcs. The incomplete data problem for three-dimensional computerized tomography, due to the very limited angular range and the small number of observers, is solved by an iterative least squares method. A theoretical example with the projection of two auroral arcs can be reconstructed with projection root-mean-square errors of the order of 1%. Application of noise deteriorates the quality of reconstruction, but with suitable low-pass filtering, root-mean-square errors of less than 5% can be obtained. The agreement between observed and calculated projections, as well as between the original and the reconstructed volume emission distribution, is quantitatively discussed for different observation geometries. With only two observation sites the range of acceptable observation geometries is limited to distances of 25 to 50 km between the observers but depends on the actual location and the morphology of the aurora. Sources of distortion of real auroral observations with intensified CCD cameras are discussed and correction procedures proposed. The complete procedure is applied to a real stereoscopic auroral observation. The correspondence of original pictures and projections of the reconstructed volume is discussed, and emission profiles along magnetic field lines are extracted from the three-dimensionally reconstructed arc.

Introduction

Auroral arcs are known to be the optical signature of acceleration processes of electrons and protons in magnetospheric regions at several thousand kilometers altitude. For a long time, ground-based optical observations, together with magnetic field and radio transmission measurements, have been the only way to examine the processes in the magnetospheric-ionospheric system. During the past decades, rockets and satellites enabled measurements well inside or near the acceleration region using instruments for field, particle, and wave measurements, but all the time, optical observations were used as an additional source of information about the actual auroral situation.

The three-dimensional phenomenon of auroral arcs was mainly studied along one-dimensional tracks of rockets or satellites or by two-dimensional studies with optical instruments and mother-daughter rocket payloads. Different attempts were made to develop a three-dimensional auroral arc model, mostly with rocket measurements and the generalization of the time series of measurements [*Margot and McNamara*, 1991]. Optical observations, so far, have been used for altitude [see, e.g., *Störmer*, 1955; *Egeland and Omhold*, 1966; *Brown et al.*, 1976] and position [see, e.g., *Kaila*, 1987; *Steen*, 1988] determination. Several examples were given for a two-dimensional emission reconstruction from rocket photometer scans [*Solomon et al.*, 1984; *McDade et al.*, 1991] and a line of ground-based meridian scanners [*Vallance Jones et al.*, 1991].

Computerized tomography is an important technique in medical diagnostics. The mathematical basis was developed by A. Cormack, who, along with G. Hounsfield, received the 1979 Nobel Prize for medicine. The main difference from our attempt of auroral tomography is that in the medical case the patients are examined in a laboratory in a known and fixed geometry between the equipment and object and that many images from various directions in a full circle around the patient are taken, either by rotation of the instrument or by an array of identical instruments [*Budinger et al.*, 1979].

Paper number 96JA01899.
0148-0227/96/96JA-01899$09.00

Auroral tomography with ground-based optical instruments is restricted to a small number of cameras, sometimes with different properties. Generally, these instruments are located on Earth and thus the angular range for observations is limited.

Emission-computed tomography in medicine has the major advantage of the quantitative determination of the moment to moment changes in the chemistry and flow physiology of injected or inhaled compounds labeled with radioactive isotopes. This advantage can be transferred to auroral tomography with the goal of a quantitative determination of temporal changes of auroral emission.

Stimulated by medical applications, different mathematical methods of quantitative evaluation of tomographic problems were developed [*Natterer,* 1986] and today, other areas of science increasingly use tomographic methods like seismology, geodesy, and electron microscopy.

Starting in the late 1980s, ionospheric tomography was used for the determination of the ionospheric electron density using radio transmission from satellites [see, e.g., *Austen et al.*, 1988; *Pryse and Kersley*, 1992] which was combined with ground-based ionospheric radar measurements [*Raymund et al.,* 1993; *Pakula et al.,* 1995; *Mitchell et al.,* 1995] to verify the results. Satellite measurements, however, suffer from the disadvantage that the periodic pass and the onset of any interesting auroral event seldom coincide.

The main advantages, neglecting the weather dependence, of ground-based optical instruments are high temporal and spatial resolution, low cost, and permanent operation. A great step into the operation of a permanent large-scale auroral observatory is the development of the multistation Auroral Large Imaging System (ALIS) in Sweden, with scientific objectives including three-dimensional (3-D) imaging of the aurora [*Steen,* 1989; *Brändström and Steen,* 1992; *Steen and Brändström*, 1993]. In a study of feasible techniques for auroral tomography [*Gustavsson,* 1992], different methods were checked using theoretical calculations with 14 ALIS stations with their optical axes pointing toward the center of the reconstruction volume. Qualitative results were discussed and given as color-coded volume representations. A similar geometry was investigated by *Pudovkin et al.* [1993] using a modified backprojection algorithm. *Aso et al.* [1990] used two cameras with overlapping fields of view but a reconstruction method with a least squares fit to a prescribed model and tested a multiplicative algebraic reconstruction technique (MART) with two to four cameras in a two-dimensional geometry [*Aso et al.,* 1993]. An iterative method was used [*Thomas and Donahue,* 1972; *Vallance Jones et al.,* 1991] for the two-dimensional reconstruction of auroral emission in an altitude-latitude plane. The combination of a single TV camera image with the data of a rocket was discussed by *Davydov and Pivovarov* [1993], but still, real three-dimensional auroral reconstruction is in the beginning state.

The aim of this paper is to describe the ability of a method to reconstruct the three-dimensional emission within an auroral arc from stereoscopic observations. As in the work by *Gustavsson* [1992], our procedure is not limited to the fit of the result to a prescribed model but the reconstruction itself needs no knowledge about the result. Furthermore, a real cone-beam observation geometry and not the idealized parallel beam geometry [*Aso et al.*, 1990] is used, the influence of noise on the results is tested, and quantitative results are given. Model calculations will be used to demonstrate the principal capacity and to discuss errors.

The result of tomographic reconstructions strongly depends on the quality of the input images. Even though astronomers use very highly developed image processing techniques to get as much information as possible [see, e.g., *Di Gesu et al.*, 1992], use of these techniques is not well documented in auroral research. Sources of distortion of real images will be discussed, and some of the astronomical image processing techniques will be used for the preparation of real images for tomographic reconstruction. At the end of this paper, results of a reconstruction from real observations will be shown.

Instrumentation and Data Analysis

The ground-based optical equipment of the Max-Planck-Institute for Extraterrestrial Physics consists of two image-intensified CCD cameras with a 150° all-sky lens with a speed of f/D=1:1.0. Out of the whole field of view our cameras use only the central part of 86° x 64°. A filter stripe enables use of different filters (we used a 557.7 nm interference filter, glass for white light, and a long-pass filter with a cutoff wavelength of 650 nm). Exact timing of the cameras is possible with integrated Global Positioning System (GPS) receivers which additionally give the exact geographical position. The images are stored on analog U-matic video tape and later digitized. Given sufficient auroral brightness, real-time observation (25 frames/s) is possible.

During a campaign in January 1995 the cameras were operated from two sites near Tromsø, Norway (Ramfjordmoen at 19.220°E and 69.584°N and Laksvatn at 19.413°E and 69.385°N), separated at a distance of 23 km. Both optical axes were directed to a point on the magnetic field line through Ramfjordmoen, observing the same field of view at approximately 100 km altitude.

Method

Given two Hilbert spaces H and K and a linear operator $\mathbf{A}$ from H into K then, the projection p of a function $f \epsilon H$ can be described by

$$p = \mathbf{A}f. \tag{1}$$

Tomography tries to solve the inverse problem [*Natterer*, 1986], given a subset of all possible $p \epsilon K$, find $f \epsilon H$ such that

$$\mathbf{A}f = p. \tag{2}$$

This problem is called well posed if it is uniquely solv-

able for each $p \epsilon K$ and if the solution depends continuously on p. Otherwise, it is called ill posed.

The properties of the aurora equal those of objects analyzed in emission-computed tomography [*Budinger et al.*, 1979], with the projection p to the center at $r = 0$ described by the integral along the individual rays r

$$p = C \int_{r=0}^{r=\infty} f(r) \exp \left\{ - \int_{s=0}^{s=r} \mu(s) ds \right\} dr. \qquad (3)$$

The parameter C contains the camera parameters like spectral sensitivity, solid angle for the observation, filter transmission, etc. The atmospheric attenuation is described by the parameter $\mu(s)$. In the visible range there is no absorption or scattering in the region of auroral emission above about 80 km. The only attenuation occurs in the lower atmosphere. This attenuation depends on the zenith angle and differs for the individual rays. As a first estimate, however, a constant attenuation can be included into the parameter C for quantitative analysis of ground-based observations. Therefore attenuation in the reconstruction volume can be neglected, simplifying the solution of the inverse problem. The volume is divided into small cubes (voxels), with the value in each voxel representing the mean of the volume emission rate $f(r)$. Thus the integral of (3) is transformed into a sum

$$p(m,n) = C \sum_{x,y,z} h_{xyz}^{mn} f(x,y,z). \qquad (4)$$

with h_{xyz}^{mn} describing the contribution of the voxel (x,y,z) to the cone region subtended by the pixel (m,n) for the two-dimensional projection $p(m,n)$ [*Katsulai and Arimizu*, 1985; *Peyrin*, 1985]. The complete procedure assumes a fixed Cartesian coordinate system for the description of the input parameters of all observers and a reference point within the object at which all cameras are looking.

All geometric calculations are simplified using homogeneous coordinates which were first developed in geometry and are now extensively used in computer graphics [*Maxwell*, 1951; *Foley and Van Dam*, 1982]. In these coordinates a point $P(x,y,z)$ is represented as $P(Wx, Wy, Wz, W)$ for any scale factor $W \neq 0$, and all three main 3-D transformations (rotation, scaling or perspective, and translation) can very conveniently be carried out as multiplications with a 4x4 matrix. This matrix is the extension of the well-known 3x3 matrix of rotations and scaling in a 3-D Cartesian coordinate system into 4-D space. The geometric correspondence between the volume elements along the line of sight and the individual image pixels (equation (4)) is calculated by matrix multiplications in homogeneous coordinates and back transformation into Cartesian coordinates by dividing by W.

The 4x4 transformation matrix is calculated by using the relative position between observer and object, the view direction, and by consideration of the perspective (cone-beam geometry). In this context the perspective describes the focal length and field of view of the optics.

Two-dimensional x, y slices of the volume are projected onto the two-dimensional image by a matrix operation, and all the individual portions of the slices with different z coordinates are summed according to (4). If necessary, the procedure would be able to correct for intrinsic absorption within the volume.

Various methods of three-dimensional reconstruction from multiple two-dimensional views have been developed and tested (for reviews, see, e.g., *Budinger and Gullberg* [1974], *Budinger et al.* [1979], *Natterer* [1986], and *Gustavsson* [1992]). None of the methods is unique and recommended to solve all problems. Rather, the methods should be checked according to the special problem, and the advantages and disadvantages must be considered.

The simplest and most rapid method of reconstruction is linear superposition or back-projection [*Budinger and Gullberg*, 1974] that reconstructs the back-projected image $B'(x,y,z)$ from a series of projections $p_l(m,n)$ as

$$B'(x,y,z) = \sum_{l,m,n} b_{mn}^{xyz} p_l(m,n) \qquad (5)$$

where for each element the contribution of each ray is summed and which passes through that element with weighting factors b_{mn}^{xyz} [*Katsulai and Arimizu*, 1985; *Peyrin*, 1985]. This back-projected image is corrected by the total density (or volume emission rate) T of the element and the total density T' of the complete array

$$B(x,y,z) = B'(x,y,z) \cdot \frac{T}{T'}. \qquad (6)$$

This method is very fast, but the agreement between the original and reconstructed three-dimensional object is bad because too many simplifications are included in this procedure.

Another class of methods are iterative or algebraic reconstruction techniques (ART) that rely on the ability to adjust the reconstructed values such that when these values are projected, the resulting projections are as close as possible to the measured data. A first estimate, like a homogeneous distribution $A^n(x,y,z)$=const, is projected, and the volume elements along each ray $k(r,\theta)$ are corrected by a factor that compensates for the discrepancy between the measured ray sum $p_{k(r,\theta)}$ and the calculated ray sum $R_{k(r,\theta)}$

$$A^{n+1}(x,y,z) = A^n(x,y,z) \cdot \frac{p_{k(r,\theta)}}{R^n_{k(r,\theta)}} \qquad (7)$$

in an iterative way for all projections from different views. The iterations can be performed in an additive or multiplicative (MART, (7)) way until a parameter

$$\lambda = \sum_v \sum_{i,j} [p(i,j) - R(i,j)]^2 \qquad (8)$$

is minimized for all views v [*Budinger and Gullberg*, 1974; *Budinger et al.*, 1979]. This method works well with a small number of projections but may require a large number of iterations until a stable solution has been found. This disadvantage increases computation time if many projections are used, like the 14 ALIS images [*Gustavsson*, 1992].

Our method combines both techniques and uses the perspective projection for the imaging of the three-

dimensional object [*Foley and Van Dam*, 1982] and the solution of the inverse transformation of a set of two-dimensional images back to a three-dimensional original object by an iterative back-projection method [*Budinger et al.*, 1979; *Natterer*, 1986]. Some of the basic routines are part of the Interactive Data Language (IDL) software package [*Research Systems, Inc.*, 1993]. The original routines RECON3 and PROJECT_VOL, however, had to be modified to correspond to the physics of the optically thin aurora and to perform the iterations and multiplicative corrections. The advantage of a combination is the decrease of computation time with the back-projection, which gives a sufficient qualitative but an inaccurate quantitative estimate of the volume emission.

The back-projection procedure calculates the geometric correspondence between the 3-D coordinates of each cell in the volume and the corresponding image x, y coordinates. The images are back-projected (5), filling one x, y slice of the volume after the other. In the zeroth iteration each cell in the volume is assigned the minimum value of the back-projected data b_{xyz} originating from the images of the observers i.

$$f^*(x, y, z) = \min[B_i'(x, y, z)]. \tag{9}$$

In the subsequent iterations we assign to each cell the value of the product of the previous cell value, with the corresponding value of the image quotient to be defined below.

With only two images the inverse problem is an incomplete data problem and extremely ill posed. According to our experimental equipment, however, we restricted this investigation to two cameras. Additionally, inverse problems tend to become unstable at the boundaries of the reconstruction volume if these boundaries limit the original object. The complete procedure tries to solve these problems with a MART-like least squares iterative method [*Natterer*, 1986].

In the procedure with theoretical data (Figure 1) the model of auroral arcs is projected in order to get the original or "exact" images p_e as the starting point for the reconstruction. Real images are transformed into these exact images by image processing. The term exact was chosen because these images are used but are not subsequently changed during the whole procedure. The zeroth iteration consists of the back-projection of these exact images and the projection of the volume in order to get the images p_k, with k=0. During all iteration steps the images p_k are compared with the exact images p_e. As input for a new back-projection, image quotients p_e/p_k are calculated. By multiplying the content of all volume elements along a ray with the corresponding value of p_e/p_k, the contents of the reconstructed volume elements are modified. After each iteration a parameter λ_k is calculated

$$\sum_{i=1}^{2}\sum_{x}\sum_{y}\sqrt{[p_e(x, y, i) - p_k(x, y, i)]^2} = \lambda_k \cdot \sum_{i=1}^{2}\sum_{x}\sum_{y} p_e(x, y, i). \tag{10}$$

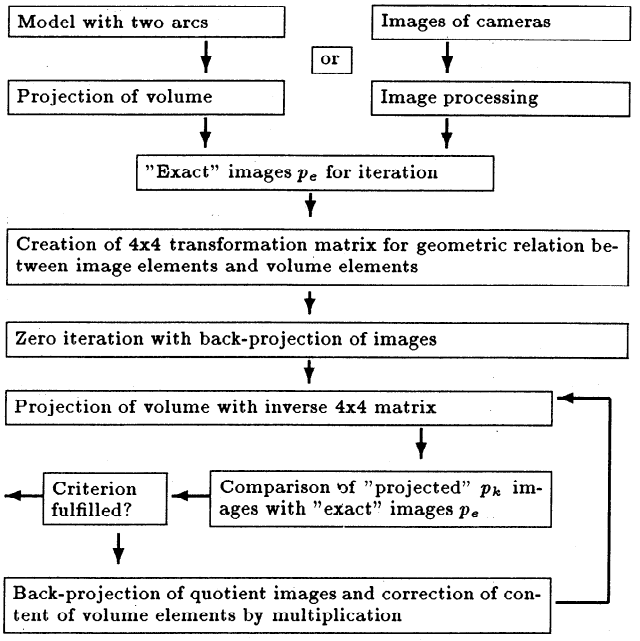

Figure 1. Flow chart for the improvement of the quantitative estimate of the volume emission by means of an iteration continued until the standard deviation between the "exact" and "projected" images becomes less than the free parameter λ. The top left part corresponds to the procedure with model calculations, while the top right part corresponds to the procedure with images from real observations.

where i is the number of images and k is the number of iterations. This parameter can be used to stop the iteration whenever a predefined value of λ_k is reached or, as was done in this study, whenever the criterion is fulfilled

$$\lambda_{k+1} \geq \lambda_k. \tag{11}$$

This parameter λ, however, is only relevant to the coincidence between the observed image and the reconstructed image. It does not guarantee the agreement between the reconstructed $f^*(x, y, z)$ and the original or "true" distribution $f(x, y, z)$ in the volume. As a quantitative check, which is possible with our theoretical modeling, a reconstruction parameter Λ is defined for the comparison of the volume data

$$\sum_{x}\sum_{y}\sum_{z}\sqrt{[f(x, y, z) - f^*(x, y, z)]^2} = \Lambda_k \cdot \sum_{x}\sum_{y}\sum_{z} f(x, y, z). \tag{12}$$

Emission-computed tomography is very much restricted by available statistics. Statistical considerations show that the root-mean-square error depends on the total number of collected events and the number of resolution elements in the reconstruction volume [*Budinger et al.*, 1979]. Unfortunately, our 8-bit system limits the total number of recorded events. Summing of sev-

eral frames is only possible as long as temporal changes during the time interval of the frames are small. Therefore and owing to calculation time reasons, we chose a 61x61x61 element reconstruction volume and resized the original 303x303 pixel pictures to a final size of 101x101.

For the demonstration of the applicability of the method a model arc was calculated in a geocentric magnetic coordinate system, with the following main assumptions [*Aso et al.*, 1990]. (1) The arc is extended in the geomagnetic east-west direction. (2) The symmetric latitudinal profile at colatitude θ is a simplified Gaussian profile

$$f_L = \exp(-\frac{(\theta - \theta_0)^2}{2\sigma^2}) \quad (13)$$

with the arc centered around a magnetic dipole field line with geomagnetic colatitude θ_0 and a latitudinal width described by the parameter σ. (3) The altitude profile is asymmetric. As an example of such an asymmetric height H dependent profile, a Chapman-type profile was chosen with the peak emission at altitude H_0

$$f_A = \exp\{1 - s(H - H_0) - \exp[-s(H - H_0)]\}. \quad (14)$$

The height extent is determined by the parameter s. The volume emission f in the arc is then the product

$$f = f_A \cdot f_L. \quad (15)$$

Results of Theoretical Modeling

Within a volume of 61x61x61 voxels, corresponding to a distance of 110 km in each direction, two auroral arcs were modeled and scaled with a factor of 255, which fits the result into an 8-bit system. The altitude of peak brightness was chosen to be at 130 km, and the Gaussian profile was calculated with a full width at half maximum (FWHM) of 4.0 km. The mean distance between the arcs was 0.35° in latitude, corresponding to 40 km. In Figure 2 the arcs are shown with their planes of 10% of maximum volume emission, together with the central magnetic field line. For the purpose of better comparability the shape of one arc was slightly changed into a more dynamic shape by applying a sinus modulation. The steps visible in the field line are due to the discrete spatial elements, with a volume emission assumed to be uniform and calculated for the central position.

These arcs were "observed" with two cameras separated by 46 km in the geomagnetic north-south direction and pointed to a reference point at 130 km altitude within the "smooth" arc. Optics with a focal length of 25 mm were used (Figure 3). The observation geometry was chosen this way so that one camera was looking along the magnetic field line of the smooth arc and the other camera was looking from the south with a parallax of 19°.

The back-projection of these images gives an estimate of the volume emission with $\lambda_0 = 0.64$ for the projection of this volume during the zeroth iteration and with $\lambda_1 = 0.18$, $\lambda_2 = 0.06$, $\lambda_3 = 0.025$, $\lambda_5 = 0.012$, and $\lambda_9 = 0.008$ during further iterations. The emission profile along the central magnetic field line of the smooth arc (Figure 4) already equals those of the original volume very well after five iterations.

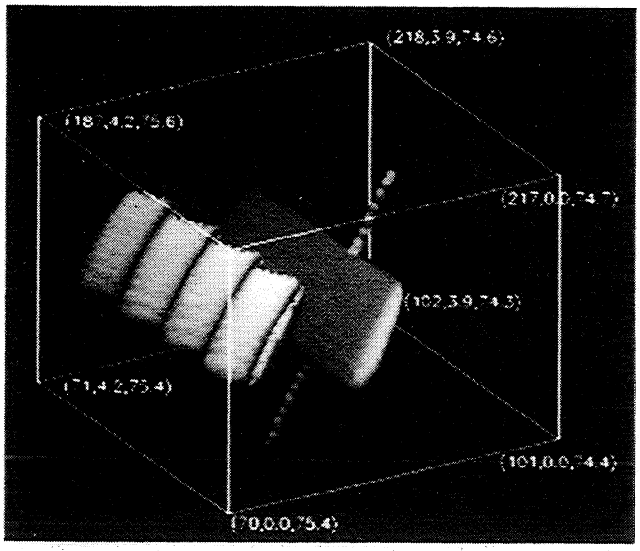

Figure 2. Model of two auroral arcs within a 61x61x61 volume shown together with the magnetic field line through the center of one arc. Each cube mark represents altitude, geocentric magnetic longitude, and geocentric magnetic latitude.

The creation of some ghost intensities in the reconstruction volume was also discussed by *Gustavsson* [1992] using 14 cameras with 60° field of view. The absolute value of these intensities is small ($\leq$ 10% of maximum volume emission), and it is caused by the incomplete data problem due to the limited angular range of observations [*Natterer*, 1986]. Possibilities to avoid such artifacts far from the main object of reconstruction would be the inclusion of a priori knowledge or the fit to some prescribed model.

The horizontal profiles (Figure 5) clarify one problem of the reconstruction with a small number of observers. While the correspondence within the arc in magnetic zenith of one station is very good (that is, one observer is looking along one main axis of the object), there are clear deviations in the arc off zenith.

Model calculations with two different observation geometries were performed as a quantitative check for the applicability of the procedure. In the first case the smooth arc was fixed at the magnetic zenith of the "main" station and the other station was moved from 110 km north to 110 km south of the main station (Figure 6a). In the second case the north-south distance between both stations was fixed at 23 km and both arcs were moved from north to south. The distance between the northern main station and the field line foot point through the smooth arc is given in Figure 6b. Calculations were performed until the iteration stopped at the smallest achievable value of λ. In addition to these values after 6-15 iterations, Figure 6 shows λ_4 after four iterations. The quality of reconstruction

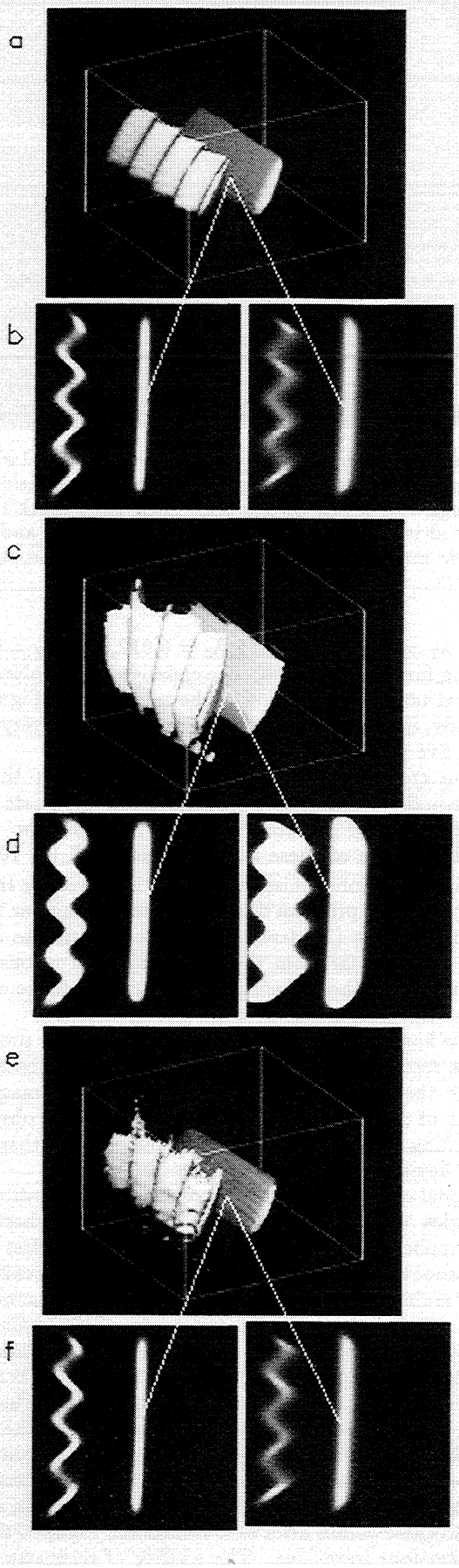

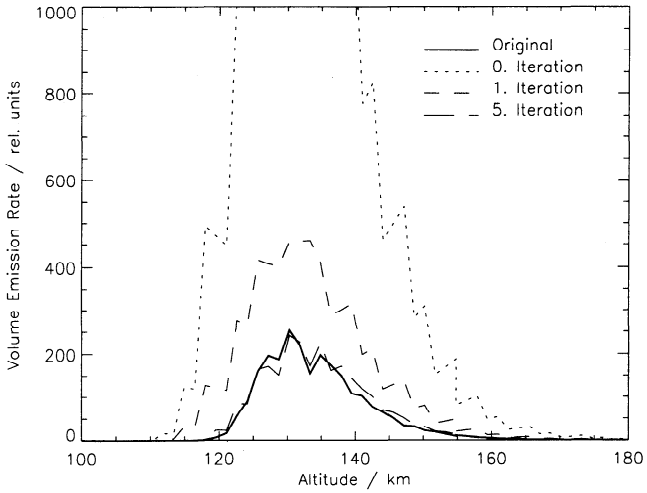

Figure 4. Emission profiles along the central magnetic field line of the theoretical arc (solid line) and along the field line in the reconstructed arc after zero (dotted line), one (short-dashed line), and five (long-dashed line) iterations.

improves, although for several geometries the iteration may be stopped after four cycles.

With the first geometry the calculation reproduces the plausible result that a good reconstruction is impossible if the distance between both stations is too small. As the magnetic field lines in the northern hemisphere are tilted toward south, a much better reconstruction can be achieved if the second station looks at the arcs from the south. The increase of the parameter λ at a south distance of $\approx$55 km is caused by the overlap of both arcs in the images of the southern station. If only one arc is modeled within the volume, a very much smaller increase of the parameter λ is obtained owing to the increasing distance.

With the second geometry, satisfactory results can be obtained as long as the main station is within 20 km of the field line foot point. Again, the increase at about 35 km distance south is caused by the overlap of both arcs in the images of the southern camera.

As the parameter λ only describes the correspondence between the images, the reconstruction parameter Λ is given in Figure 7. All conclusions discussed concerning Figure 6 apply. Additionally, a good reconstruction is obtained as long as the smooth arc is in or between the magnetic zeniths of the cameras. Our special example

Figure 3. Illustration of the iteration process for reconstructing the volume with two model arcs (a). Two observers are separated by 46 km in the north-south direction and are looking along the field line and with a parallax of 19°, respectively (b). The zeroth iteration (c) yields a rough estimate of the geometry, a much too high estimate of the volume emission, and much too bright images (d) of this volume with $\lambda_0 = 0.64$. Further iterations yield $\lambda_1 = 0.18, \lambda_2 = 0.06, \lambda_3 = 0.025$, and $\lambda_4 = 0.016$. The result (e) of the sixth iteration fulfills the criterion with $\lambda \leq 0.01$ (f).

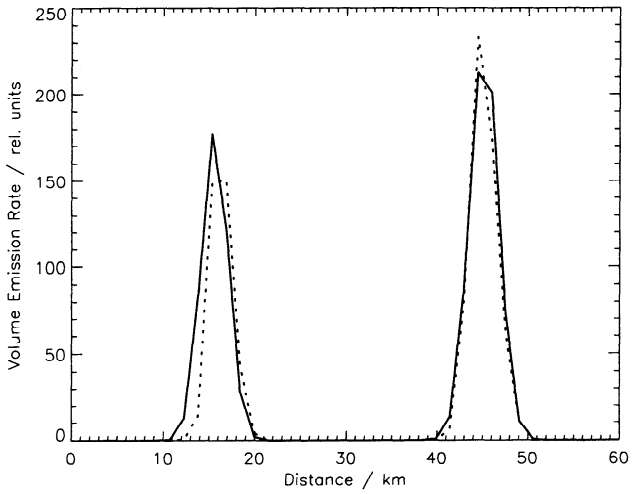

Figure 5. Horizontal emission profiles perpendicular to the theoretical arcs (solid line) and through the reconstructed arcs after nine iterations (dotted line).

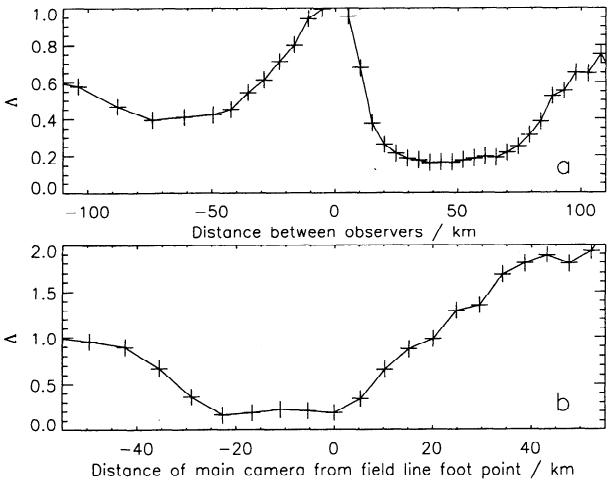

Figure 7. Reconstruction parameter Λ for the two different observation geometries described in Figure 6.

of two parallel arcs at 40 km distance inhibits much better results in Figure 7b because one arc is always off zenith. If only one arc is used, reconstruction parameters Λ as low as 1/3 of the values given in Figure 7 are obtained. This agrees with the conclusions given by *Natterer* [1986] that homogeneous objects can be reconstructed from very few views and a very small angular range. On the other hand, this confirms that a good reconstruction of very dynamic auroral structures like curls or spirals may be impossible.

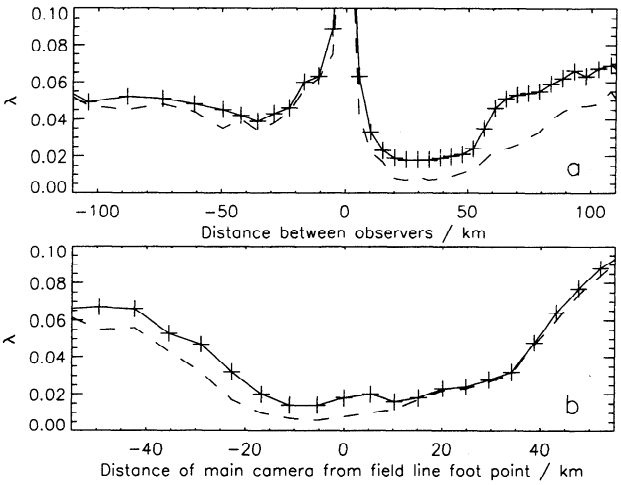

Figure 6. Quality parameter λ for two different observation geometries. (a) The "smooth" arc is fixed at the magnetic zenith of the "main" station, and the other station moves from 110 km north (negative distance) to 110 km south. The dashed line connects the minimum values of λ achieved after 6-15 iteration steps. The solid line connects the points of λ_4. (b) Both stations are fixed at a distance of 23 km, and the arcs move from north to south. The distance between the northern main station and the foot point of the field line through the smooth arc is given.

These results correspond qualitatively to the results of two-dimensional MART reconstruction of one auroral arc given by *Aso et al.* [1993]. Unfortunately, in their figures the profile difference is not explicitly described and cannot be compared to our quantitative results.

The influence of noise on the quality of reconstruction was tested with a Gaussian additive noise. As a very general case, two independent noise components n_1 and n_2 were calculated and the content of each image pixel I_i after projection of the original volume was changed into I_i^*

$$I_i^* = I_i + n_1 \cdot I_i + n_2. \tag{16}$$

This procedure corresponds to the use of camera images with a distorted projection due to technical effects like the use of an image intensifier and read-out noise of a CCD. Figure 8 shows a logarithmic representation of the original image without noise and the image with the noise added. The reconstruction with these images in an ideal observation geometry converges much slower, and the comparison of the images never reaches values of $\lambda \leq 0.05$. Application of a Fourier low-pass filter improves convergence to $\lambda_3 = 0.049$ and a minimum of $\lambda_8 = 0.035$ (Figure 9) and to a minimum of $\lambda_6 = 0.048$ with a median filter.

Reconstruction of Real Observations

Image Processing Before Reconstruction

Real images taken with cameras are subject to geometry, sensitivity, background, and noise distortions. Furthermore, extraction of real coordinates from images needs to consider the projection of the celestial sphere to the plane of the CCD chip.

The main noise source of our images is due to the statistical nature of the intensification process in the microchannel plate. Calibration images taken with a homogeneous light source were used to determine the noise level for areas of homogeneous brightness, and the real images were filtered with a Fourier low-pass filter.

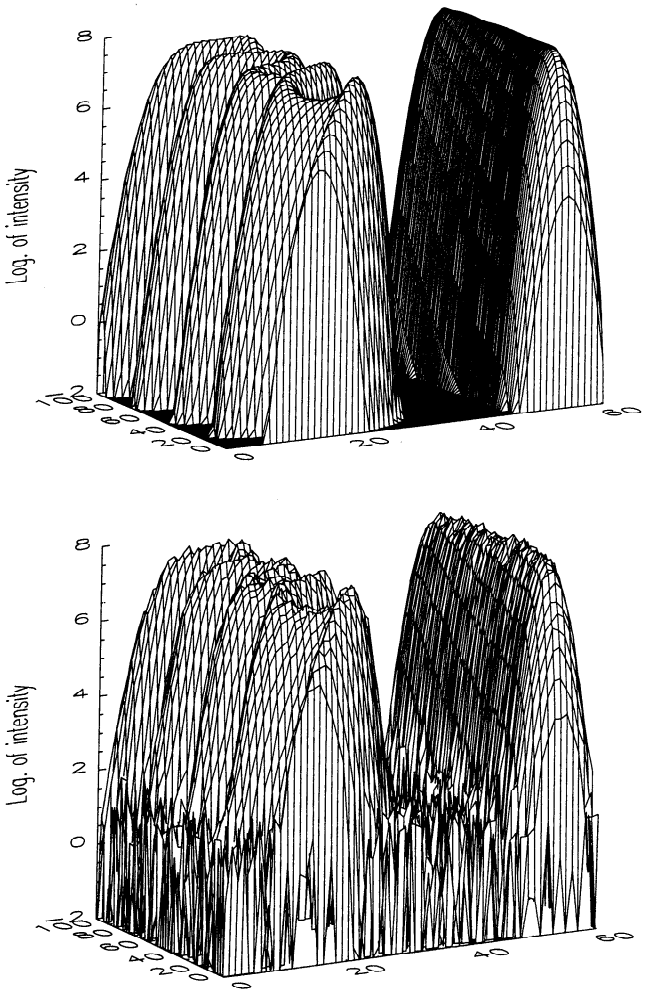

Figure 8. Logarithmic representation of the intensity (top) in the original image and (bottom) after the addition of noise. A pixel content of 0 was set to e^{-2}.

The geometry distortions in our images are mainly due to the optical properties of the all-sky optics and the optical tapers in the cameras. A computer program was written to correct these distortions by means of a least squares fitted third-degree polynomial. After identification of the night sky area and a first estimate of the celestial coordinates of the image center [*Smart*, 1965], this program projects catalogue stars into the image. The actual positions of the stars have to be given with the computer mouse, and the centroid of the real position is calculated. With a set of 30-50 stars within the calibration image (sometimes produced by summation of several frames) the exact celestial coordinates of the image center, rotation angle between sky north direction and image axis, and radial scale are calculated, together with the polynomial. Partly, this method equals those of *Kaila* [1987].

The nonuniform sensitivity of the cameras is corrected with the flat-fielding procedure [*King*, 1986]. The following two different ways were chosen: first, use of the calibration images taken with our light standard, and second, use of the night sky. The disadvantage of the first way is that only the camera without the all-sky optics can be calibrated in our standard. In the second method it is hard to find a homogeneous "flat" sky, especially in the polar regions of the auroral oval. By "vertical" median filtering (i.e., median of each pixel over all frames) of a time set of clear sky images, the stars are deleted and only the radial sensitivity and "bad pixels" are conserved.

The sky background is also determined with a vertical median filtering technique. However, while the sensitivity is a multiplicative correction, the background is subtracted from the images.

The last step of our image-processing procedure is sharpening of the structures by deconvolution of the point-spread function [*Di Gesu et al.*, 1992]. The point-spread function is assumed as a two-dimensional Gaussian profile and determined with several reference stars. While most astronomical CCD cameras have near- symmetric point-spread functions in the x and y directions of the images caused by the properties of the optics only, our images have a strong asymmetry. The reason is the digitization of the images from analog video tape. While the pixels in the y direction are not correlated by the read-out process, the pixels in the x direction are more correlated, yielding a larger width in the x than in the y direction. Image enhancement is then done as a deconvolution with a maximum-likelihood iteration [*Research Systems, Inc.*, 1993]. The effect of this deconvolution is small for wide-angle images but becomes important for tele-images.

Reconstruction With Real Images

The most critical factors influencing reconstruction with real images are background subtraction, noise reduction, geometry correction, and sensitivity calibration. The cutoff frequency of low-pass Fourier filtering has to be chosen very carefully in order to obtain satisfactory results. Different camera sensitivities have to be corrected (in our case there was 25% difference). Another problem may be the exact determination of the

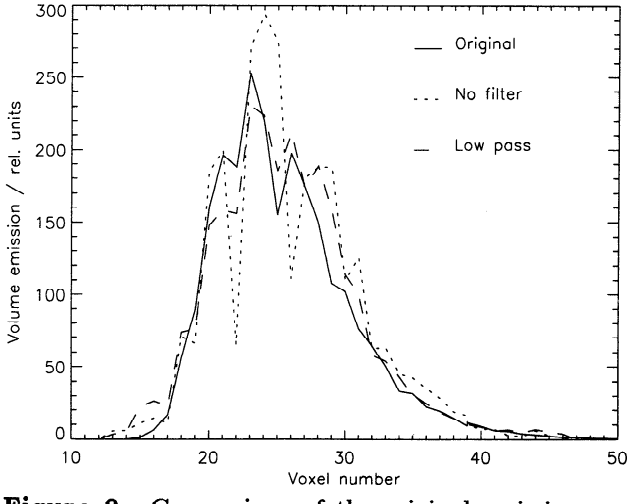

Figure 9. Comparison of the original emission profile (solid line) with the profile extracted from the arc reconstructed with the noisy images (dotted line) and after Fourier low-pass filtering of the images (dashed line).

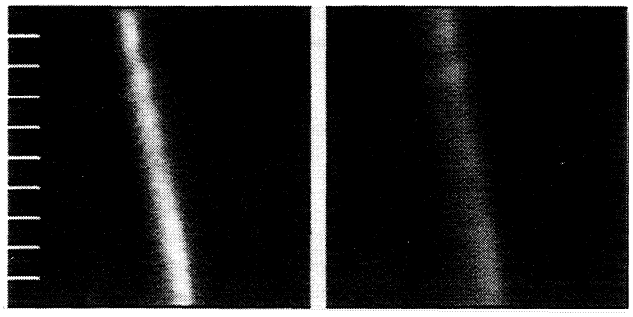

Figure 10. Pictures of the aurora taken by two cameras in Norway on January 30, 1995. Wide-angle optics and a long-pass red filter were used. The size of the image corresponds to about 80x80 km^2 at 110 km altitude. The short lines in the left image mark the positions of the profiles of Figure 11.

reference point in all images. Improper location within different images would result in a smearing of any substructure. This is not a big problem with our two cameras with intersecting optical axes but may become a problem with more images.

Figure 10 shows two images after image processing used for reconstruction. Both images were taken with a long-pass blocking filter with a cutoff wavelength at 650 nm, thus registering mostly the prompt emission of the first positive band of N_2 and the Meinel band of N_2^+. The 4x4 transformation matrix was calculated according to the locations of the observation sites. The procedure converges to a stable solution after five iterations with $\lambda_5 = 0.17$ (Figure 11). The profiles extracted at 15-km distant positions along the arc center in the east-west direction (Figure 12) represent the local differences of the excitation. The small parallax of only 11° inhibits much better convergence. Theoretical modeling

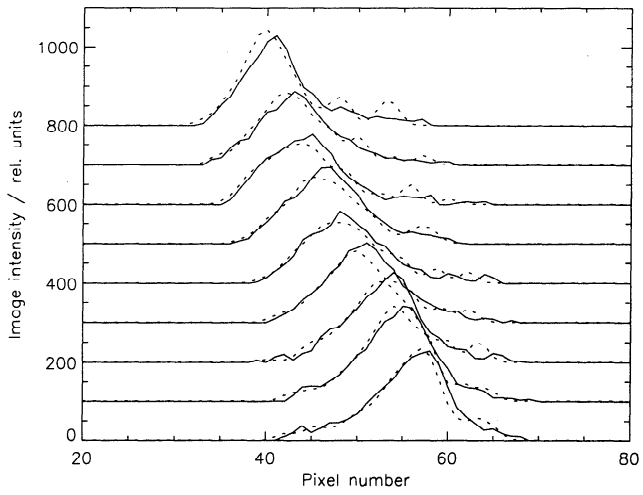

Figure 11. Intensity profiles through the original image of one observer in Norway (solid line, Figure 10) and profiles through the corresponding positions in the projection after five iterations (dotted line). For the purpose of better comparability the profiles are shifted by 100 intensity steps.

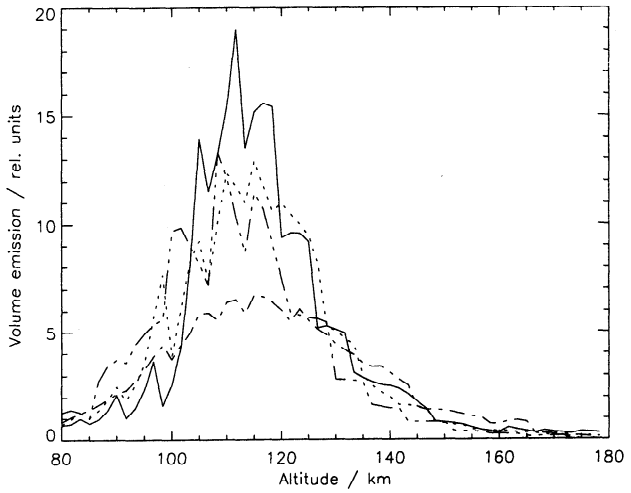

Figure 12. Emission profiles along magnetic field lines extracted at a distance of 15 km along the auroral arc observed in Norway on January 30, 1995.

with one arc provided a minimum of the parameter λ at observer distances between 30 and 40 km, and these images were taken with a distance of 23 km, but the result is, nevertheless, satisfactory. A three-dimensional representation of the relative volume emission is given in Figure 13. The mean thickness of the arc (FWHM) was 4-7 km.

Conclusions

The proposed iterative method solves the ill-posed problem of reconstruction from two images. The algorithm with an auroral arc model can be used to estimate the accuracy that is feasible with incomplete data of limited angles and to study the influence of noise on the quality of reconstruction. Furthermore, various locations of observers can be tested for the opti-

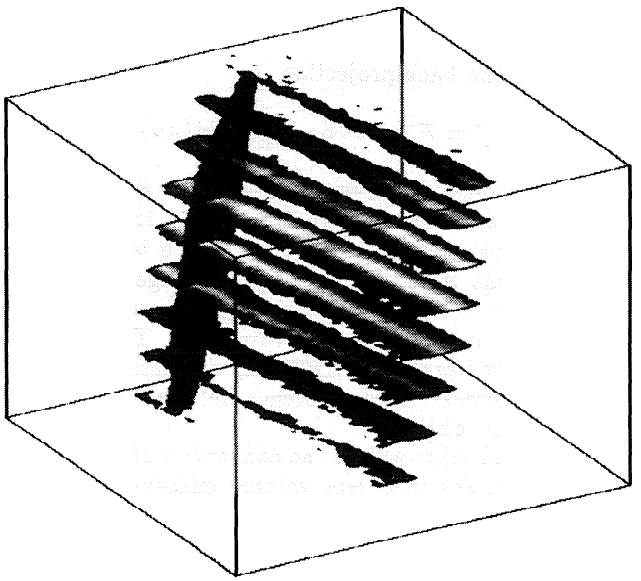

Figure 13. Three-dimensional representation of the relative volume emission within the auroral arc observed in Norway on January 30, 1995.

mization of observation conditions before observation campaigns, and different theoretical altitude profiles of auroral emission can be checked.

Three-dimensional reconstruction of auroral emission is possible with the presented iterative procedure of perspective projection and back-projection of the images. Especially, the procedure is unique and not restricted to a special prescribed model or a special auroral type. Best results are obtained with the auroral arc within about 5° of magnetic zenith of one observer, but an arc moving from the zenith of one observer to the zenith of the other still provides sufficient accuracy of the reconstruction procedure for studying temporal changes. In the case of two parallel arcs, at least one observer has to look "through" the arcs. The procedure can be used to investigate the reconstruction of much broader (inverted-V like) arcs, of parallel arcs with smaller distances, and of smaller structures than have been studied here. The complete procedure of reconstruction and projection with eight iterations takes about 15 min on a Digital Equipment Corporation (DEC) 3000 computer.

For the test of the procedure, real images had to be used that were taken in an unfavorable observation geometry. Nevertheless, the auroral arc could be reconstructed and reasonable altitude profiles could be obtained. Future observation campaigns will use the predictions of the theoretical calculations for a proper selection of observation locations.

The reconstruction with images taken in white light sometimes show profiles which can be interpreted as the sum of emission profiles of different species/wavelengths as in the work by *Davydov and Pivovarov* [1993]. A peak of maximum emission could generally not be found, but rather, an altitude range of constant emission was evident.

Further work will be done to use the filtered back-projection method [*Budinger et al.*, 1979] with the two different algorithms of back-projection of filtered projections

$$f = \text{back project}\{\mathcal{F}^{-1}[\tilde{c}\mathcal{F}(p)]\} \tag{17}$$

or filter of the back-projection

$$f = \mathcal{F}^{-1}\{\tilde{c}\mathcal{F}[\text{back project}(p)]\}. \tag{18}$$

$\mathcal{F}^{1,-1}$ symbolizes the forward and inverse Fourier transformation, and $\tilde{c}$ is a filter function in the frequency domain. This method works well with a large number of projections from the full angular range around the object under study, but the accuracy of reconstruction decreases with the number of projections. The combination with the iterative MART may decrease computing time and increase correspondence between original and reconstructed object.

Additional tasks will be the conversion of the relative emission profiles into real volume emission rates and the comparison with electron density profiles measured along the magnetic zenith with the European Incoherent Scatter UHF-radar. A test of the procedure with a set of ALIS images is a further interesting prospect.

Acknowledgments. The authors are grateful to the two referees for extremely helpful remarks. The Editor thanks two referees for their assistance in evaluating this paper.

References

Aso, T., T. Hashimoto, M. Abe, T. Ono, and M. Ejiri, On the analysis of aurora stereo observations, *J. Geomagn. Geoelectr., 42,* 579–595, 1990.

Aso, T., K. Muguruma, T. Yabu, T. Hashimoto, M. Abe, and M. Ejiri, A note on the computed auroral tomography by the MART method, *Sci. Rep. 213,* pp. 23–33, Inst. för Rymdfysik, Kiruna, Sweden, 1993.

Austen, J. R., S. J. Franke, and C. H. Liu, Ionospheric imaging using computerized tomography, *Radio Sci., 23,* 299–307, 1988.

Brändström, U., and Å. Steen, Report on the ALIS project, *Sci. Rep. 209,* pp. 310–321, Inst. för Rymdfysik, Kiruna, Sweden, 1992.

Brown, N. B., T. N. Davis, T. J. Hallinan, and H. C. Stenbaek-Nielsen, Altitude of pulsating aurora determined by a new instrumental technique, *Geophys. Res. Lett., 3,* 403–404, 1976.

Budinger, T. F., and G. T. Gullberg, Three-dimensional reconstruction in nuclear medicine emission imaging, *IEEE Trans. Nucl. Sci., NS-21*(3), 2–20, 1974.

Budinger, T. F., G. T. Gullberg, and R. H. Huesman, Emission computed tomography, in *Image Reconstruction From Projections,* Springer-Verlag, New York, 1979.

Davydov, V. S., and V. V. Pivovarov, Test of auroral tomography methods for the ALIS project, *Sci. Rep. 213,* pp. 59–62, Inst. för Rymdfysik, Kiruna, Sweden, 1993.

Di Gesu, V., L. Scarsi, R. Buccheri, P. Crane, M. C. Maccarone, and H. U. Zimmermann (Eds.), *Data Analysis in Astronomy IV,* Plenum, New York, 1992.

Egeland, A., and A. Omhold, Carl Störmers height measurements of aurora, *Geophys. Publ., 26,* 1–12, 1966.

Foley, J. D., and A. Van Dam, *Fundamentals of Interactive Computer Graphics,* Addison-Wesley, Reading, Mas., 1982.

Gustavsson, B., A study of feasible tomographic inversion techniques for ALIS, *Tech. Rep. 39,* Inst. för Rymdfysik, Kiruna, Sweden, 1992.

Kaila, K. U., An iterative method for calculating the altitudes and positions of auroras along the arc, *Planet. Space Sci., 35,* 245–258, 1987.

Katsulai, H., and N. Arimizu, An iterative reconstruction from truncated projection data, *IEEE Trans. Nucl. Sci., 32*(3), 1217–1224, 1985.

King, I. R., Cluster photometry: Present state of the art and future developments, in *Data Analysis in Astronomy II,* edited by V. Di Gesu, L. Scarsi, P. Crane, J. H. Friedman, and S. Levialdi, pp. 17–35, Plenum, New York, 1986.

Margot, J., and A. G.McNamara, Comparison of plasma-density and electron-temperature profiles during the auroral modelling campaign ARIES, *Can. J. Phys., 69,* 950–958, 1991.

Maxwell, E. A., *General Homogeneous Coordinates in Space of Three Dimensions,* Cambridge Univ. Press, New York, 1951.

McDade, I. C., N. D. Lloyd, and E. J. LLewellyn, A rocket tomography measurement of the N_2^+ 3914 Å emission rates within an auroral arc, *Planet. Space Sci., 39,* 895–906, 1991.

Mitchell, C. N., D. G. Jones, L. Kersley, S. E. Pryse, and

I. K. Walker, Imaging of field-aligned structures in the auroral ionosphere, *Ann. Geophys., 13,* 1311–1319, 1995.

Natterer, F., *The Mathematics of Computerized Tomography,* John Wiley, New York, 1986.

Pakula, W. A., P. F. Fougere, J. A. Klobuchar, J. J. Kuenzler, M. J. Buonsanto, J. M. Roth, J. C. Foster, and R. E. Sheehan, Tomographic reconstruction of the ionosphere over North America with comparison to ground-based radar, *Radio Sci., 30,* 89–103, 1995.

Peyrin, F. C., The generalized back projection theorem for cone beam reconstruction, *IEEE Trans. Nucl. Sci., 32*(4), 1512–1519, 1985.

Pryse, S. E., and L. Kersley, A preliminary experimental test of ionospheric tomography, *J. Atmos. Terr. Phys., 54,* 1007–1012, 1992.

Pudovkin, M. I., V. N. Troyan, and G. A. Ryzhikov, Tomography reconstruction of a 3D-auroral luminosity distribution, *Sci. Rep. 213,* pp. 83–102, Inst. för Rymdfysik, Kiruna, Sweden, 1993.

Raymund, T. D., S. E. Pryse, L. Kersley, and J. A. T. Heaton, Tomographic reconstruction of ionospheric electron density with European incoherent scatter radar verification, *Radio Sci., 28,* 811–817, 1993.

Research Systems, Inc., *IDL User's Guide,* Boulder, Colo., 1993.

Smart, W. M., *Text-Book on Spherical Astronomy,* Cambridge Univ. Press, New York, 1965.

Solomon, S. C., P. B. Hays, and V. J. Abreu, Tomographic inversion of satellite photometry, *Appl. Opt., 23,* 3409–3414, 1984.

Steen, Å., An auroral height measuring system designed for real time operations, *Rev. Sci. Instrum., 59,* 2211–2219, 1988.

Steen, Å., ALIS - An auroral large imaging system in northern Scandinavia, *Eur. Space Agency Spec. Publ. ESA SP-291,* 299-303, 1989.

Steen, Å., and U. Brändström, A multi-station ground-based imaging system at high latitudes, *STEP Int. Newsl., 3,* 1993.

Störmer, C., *The Polar Aurora,* Clarendon, Oxford, 1955.

Thomas, R. J., and T. M. Donahue, Analysis of Ogo 6 observations of the O I 5577-A tropical nightglow, *J. Geophys. Res., 77,* 3557–3567, 1972.

Vallance Jones, A., et al., The ARIES auroral modelling campaign: Characterization and modelling of an evening auroral arc observed from a rocket and a ground-based line of meridian scanners, *Planet. Space Sci., 39,* 1677–1705, 1991.

O.H. Bauer, H.U. Frey, S. Frey, and G. Haerendel, Max-Planck-Institut für extraterrestrische Physik, D-85740 Garching, Germany. (e-mail: ohb@mpe-garching.mpg.de; hfr@mpe-garching.mpg.de; saf@mpe-garching.mpg.de; hae@mpe-garching.mpg.de)

D.J. Carr, Research Systems, Inc., 2995 Wilderness Place, Suite 203, Boulder CO 80301, (e-mail: dan@rsinc.com)

(Received December 22, 1995; revised May 6, 1996; accepted June 10, 1996.)